Biomaterials Advances 154 (2023) 213589

Contents lists available at ScienceDirect

Biomaterials Advances

journal homepage: www.journals.elsevier.com/materials-science-and-engineering-c

Sustained growth factor delivery from bioactive PNIPAM-*grafted*-chitosan/heparin multilayers as a tool to promote growth and migration of cells

Yi-Tung Lu [a], Pei-Tzu Hung [a], Kui Zeng [b], Matthias Menzel [c], Christian E.H. Schmelzer [d], Kai Zhang [b], Thomas Groth [a,d,*]

[a] Department of Biomedical Materials, Institute of Pharmacy, Martin Luther University Halle-Wittenberg, Heinrich-Damerow-Strasse 4, 06120 Halle, Saale, Germany
[b] Sustainable Materials and Chemistry, Dept. Wood Technology and Wood-based Composites, University of Göttingen, Büsgenweg 4, D-37077 Göttingen, Germany
[c] Department of Biological and Macromolecular Materials, Fraunhofer Institute for Microstructure of Materials and Systems (IMWS), Walter-Hülse-Str. 1, 06120 Halle, Saale, Germany
[d] Interdisciplinary Center of Material Research, Martin Luther University Halle-Wittenberg, Heinrich-Damerow-Strasse, 06120 Halle, Saale, Germany

ARTICLE INFO

Keywords:
Poly(*N*-isopropylacrylamide)
FGF-2 delivery
Vitronectin adsorption
Layer-by-layer technique
Glycosaminoglycan
Stem cell culture

ABSTRACT

Delivery of growth factors (GFs) is challenging for regulation of cell proliferation and differentiation due to their rapid inactivation under physiological conditions. Here, a bioactive polyelectrolyte multilayer (PEM) is engineered by the combination of thermoresponsive poly(*N*-isopropylacrylamide) (PNIPAM) and glycosaminoglycans to be used as reservoir for GF storage. PNIPAM-*grafted*-chitosan (PChi) with two degrees of substitution (DS) are synthesized, namely LMW* (DS 0.14) and HMW (DS 0.03), by grafting low (2 kDa) and high (10 kDa) molecular weight of PNIPAM on the backbone of chitosan (Chi) to be employed as polycations to form PEM with the polyanion heparin (Hep) at pH 4. Subsequently, PEMs are chemically crosslinked to improve their stability at physiological pH 7.4. Resulting surface and mechanical properties indicate that PEM containing HMW is responsive to temperature at 20 °C and 37 °C, while LMW is not. More importantly, Hep as terminal layer combined with HMW allows not only a better retention of the adhesive protein vitronectin but also a sustained release of FGF-2 at 37 °C. With the synergistic effect of vitronectin and matrix-bound FGF-2, significant promotion on adhesion, proliferation, and migration of 3T3 mouse embryonic fibroblasts is achieved on HMW-containing PEM compared to Chi-containing PEM and exogenously added FGF-2. Thus, PEM containing PNIPAM in combination with bioactive glycosaminoglycans like Hep represents a versatile approach to fabricate a GF delivery system for efficient cell culture, which can be potentially served as cell culture substrate for production of (stem) cells and bioactive wound dressing for tissue regeneration.

1. Introduction

Cell behaviors during medical application of implants is triggered by the interaction with the biomaterial surface and related protein adsorption, cell-cell contacts and soluble bioactive molecules [1]. The latter are represented for example by fibroblast growth factor-2 (FGF-2) that acts as stimulator to promote proliferation and migration of fibroblasts and endothelial cells important for wound healing, and neovascularization, but also related to the maintenance of self-renewal and proliferation of human pluripotent stem cells (hPSC) [2–4]. By binding to transmembrane FGF receptors (FGFR), FGF-2 activates intracellular signaling cascades including Rho family of small GTPases, and mitogen-

Abbreviations: Chi, chitosan; CLSM, confocal laser scanning microscopy; DS, degrees of substitution; DMEM, Dulbecco's modified Eagle's medium; ECM, extracellular matrix; EDC, 1-ethyl-3-(3-dimethylaminopropyl) carbodiimide; ERK, extracellular signal-regulated kinase; ELISA, enzyme-linked immunosorbent assay; FGF-2, fibroblast growth factor-2; FGFR, fibroblast growth factor receptor; FITC, fluorescein isothiocyanate; FI, fluorescence intensity; FBS, fetal bovine serum; GF, growth factor; GAG, glycosaminoglycans; HMW, high molecular weight; Hep, heparin; hPSC, human pluripotent stem cells; LMW, low molecular weight; LbL, layer-by-layer; LCST, lower critical solution temperature; NHS, *N*-hydroxysuccinimide; MAPK, mitogen-activated protein kinase; PEI, polyethyleneimine; PBS, phosphate-buffered saline; PEM, polyelectrolyte multilayer; PNIPAM, poly(*N*-isopropylacrylamide); PChi, PNIPAM-*grafted*-Chi; PI3K, phosphatidylinositol 3-kinase; PE, polyelectrolyte; TCPS, tissue culture polystyrene; VN, vitronectin.

* Corresponding author at: Department of Biomedical Materials, Institute of Pharmacy, Martin Luther University Halle-Wittenberg, Heinrich-Damerow-Strasse 4, 06120 Halle, Saale, Germany.
E-mail address: thomas.groth@pharmazie.uni-halle.de (T. Groth).

https://doi.org/10.1016/j.bioadv.2023.213589
Received 22 May 2023; Received in revised form 4 August 2023; Accepted 13 August 2023
Available online 14 August 2023

activated protein kinase/extracellular signal-regulated kinase (MAPK/ERK) [5]. Specially, these signal transductions can be activated by cooperation of FGFR and cell adhesion molecule integrins (e.g. $\alpha_V\beta_3$) to regulate cell adhesion and spreading [6,7]. FGF-2 is generally supplemented to the culture medium to support cell growth [8]. However, the issues about its short half-life (22–29 h) under physiological environments must be addressed and the local concentration must be well controlled to avoid inhibition of proliferation or differentiation of stem and other cells [9,10]. Sulfated glycosaminoglycans (GAGs) have high affinity to proteins with GAG-binding domains such as extracellular matrix (ECM) proteins (e.g. fibronectin, vitronectin) and GFs (e.g. FGF-2, TGF-β), but also act as a storage reservoir to protect GFs from proteolytic digestion [11,12]. GAGs like heparin (Hep) added to culture media have shown to improve the stability and prolong the half-life of FGF-2 [13]. Therefore, engineering an appropriate delivery system involving GAGs is attractive to prolong the activity of GF like FGF-2 to achieve the desired cell and tissue response.

Layer-by-layer (LbL) assembly has emerged as a facile and cost-effective technique to fabricate biocompatible and bioactive surfaces using negatively charged GAGs for making GFs delivery systems [2,14,15]. By alternating deposition of materials, it is mainly depending on ion pairing between oppositely charged polyelectrolytes (PEs) to form a polyelectrolyte multilayer (PEM) [16]. The physical and mechanical properties of the PEM are based on the nature of selected PE and environmental conditions (e.g., pH, ionic strength, and temperature) [16]. Chitosan (Chi) is widely used as polycation regarding its biocompatibility, abundancy and anti-bacterial properties [17,18]. Multiple studies have reported the use of PEMs as reservoirs for protecting GFs from degradation and prolonging their long-term presentation. For example, loading FGF-2 on PEMs composed of Hep and Chi enhanced the mitogenic activity of mesenchymal stem cells [19]. Another advantage of PEM is that the locally released concentration of GFs can be controlled by chemical crosslinking of the PEM that also improves their stability and modulates their physiochemical properties. In this regard, it was shown previously that delivery of bone morphogenetic protein-2 and FGF-2 from crosslinked PEMs exhibited the ability to induce osteogenic differentiation of myoblasts and promote migration and growth of fibroblasts for wound healing and culture of adipose derived stem cells, respectively [2,14,20].

Utilizing LbL technique facilitates engineering of PEMs containing poly(*N*-isopropylacrylamide) (PNIPAM) and has been demonstrated the ability to thermally control protein adsorption or drug delivery such as anti-COVID-19 drug Favipiravir [21–23]. PNIPAM is thermoresponsive and widely applied for drug delivery and cell sheet engineering owing to its lower critical solution temperature (LCST) ≈ 32 °C close to the physiological temperature [24]. Below 32 °C, the hydrophilic amide groups are dominant making the polymer highly hydrated, soluble in aqueous solution and repellent to proteins and cells. Its hydrophobic isopropyl groups govern when temperature rises above 32 °C, and lead to the dehydration of the polymer due to the hydrophobic interaction that aids protein adsorption and supports cell adhesion [25,26]. The collapsed PNIPAM becomes a gel to entrap drugs inside the matrix and allow their slow release through the hydrophobic interaction between drugs and PNIPAM [27,28]. PNIPAM has shown a great ability to retain GF activity and sustain their release to promote cell proliferation and differentiation [28–30]. However, the application of PNIPAM-containing PEM for GF delivery in tissue engineering is rarely found due to the lacking anchoring sites of PNIPAM for cells causing inferior cell adhesion [21,23,31]. Thus, a novel approach for enhancing the bioactivity of PNIPAM-containing PEM is desired to regulate cell behaviors.

Our previous study has investigated the ability of a combination of bioactive Hep and PNIPAM-*grafted*-chitosan (PChi) to form a stable PEM upon crosslinking under physiological pH 7.4, and modulate the physical properties in response to temperature (i.e. wettability) related to the biocompatibility and adhesion of stem cells [32]. In this current study, the effect of temperature on the mechanical properties of PChi-containing PEMs is further studied which may affect protein adsorption and cell behaviors. Vitronectin (VN) as an adhesive protein can promote cell adhesion via the specific binding of cell integrin $\alpha_V\beta_3$ and $\alpha_V\beta_5$ [33]. The bioactivity of PChi or Hep terminated PEMs is interesting for the interaction with VN in response to temperature. FGF-2 and VN have been reported to regulate particularly hPSC responses cooperatively [4,6,34]. The synergistic bioactivity of VN and FGF-2 was assessed here using 3T3 mouse embryonic fibroblasts regarding cell adhesion, migration, and growth. The final goal is to achieve a sustained bioactivity of FGF-2 loaded on these PEMs towards cells, important for future applications in effective culture and large-scale expansion of stem cells that may be superior to use of soluble FGF-2 supplemented in culture medium.

2. Materials and methods

2.1. Materials

Chitosan (deacetylation degree ≥92.6 %, 40–150 kDa) was purchased from HMC Heppe Medical Chitosan GmbH (Halle, Germany). Heparin sodium salt (sulfation degree = 1.06, 8–25 kDa) and 1-ethyl-3-(3-dimethylaminopropyl) carbodiimide (EDC) was obtained from Thermo Fisher (Kandel) GmbH (Karlsruhe, Germany). Polyethyleneimine (PEI, 750 kDa), *N*-hydroxysuccinimide (NHS), carboxylic acid−terminated PNIPAM (PNIPAM-COOH, 2 and 10 kDa) and fluorescein isothiocyanate (FITC) were provided by Sigma-Aldrich Chemie GmbH (Steinheim, Germany). *n*-Hexane and tetrahydrofuran (THF) were derived from Th. Geyer GmbH & Co. KG (Renningen, Germany). Recombinant human vitronectin (VN) was purchased from PeproTech, Inc. (Hamburg, Germany). FGF-2 (recombinant human FGF-basic FGF) and ELISA kit were obtained from PeproTech, Inc. (New Jersey, USA).

2.2. Synthesis and characterization of PNIPAM-grafted-chitosan

PNIPAM-*grafted*-chitosan (PChi) was synthesized as described previously [32]. Briefly, at 25 °C, the carboxylic groups of PNIPAM-COOH was activated by EDC/NHS to form amide bond with the amino groups located at C2 − position of Chi. Initially, Chi and PNIPAM-COOH (2 or 10 kDa) were separately dissolved in 2 % acetic acid solution. The PNIPAM-COOH solution was reacted for 1 h by adding EDC and NHS followed by mixing with Chi solution to steadily stir overnight at 25 °C. Afterwards, the mixed solution was precipitated in a THF/*n*-hexane solution (4:1) and purified with dialysis membrane (MWCO: 12,000 − 14,000) against Milli-Q water for one week. Finally, the pure PChi was lyophilized by freeze dryer (ALPHA 1–2 LDplus, Christ, Osterode am Harz, Germany). Using weight ratio of Chi/PNIPAM = 1:3 and the molar ratio of repeating unit of Chi/EDC/NHS = 1:3:1.5, the degrees of substitution (DS) of PNIPAM grafted to Chi were characterized by ^{1}H NMR in our previous study [32]. PChi with DS of 0.14 and 0.03 achieved from 2 kDa and 10 kDa of PNIPAM-COOH were named as LMW* and HMW, respectively.

2.3. Multilayer formation by layer-by-layer technique

Glass cover slips (Ø 12 mm, Menzel, Braunschweig, Germany) were cleaned with 25 % NH_4OH, 35 % H_2O_2, and micropure water (1:1:5, v/v/v) at 80 °C for 15 min. Afterwards, the samples were washed with micropure water for 6 × 5 min and dried with nitrogen stream.

The PEM were assembled manually by pipetting solutions of PE applying the same procedure as in previous studies of our and other groups [35,36], for cleaned glass cover slips and tissue culture polystyrene (TCPS) as substrates used for atomic force microscopy and biological investigations, respectively. PEI as the first anchoring layer was coated to achieve a positive charge on the substrate. The following layers were deposited with two bilayers of polyanion Hep and

polycation Chi to achieve a basal multilayer without PNIPAM. Subsequently, PChi replaced Chi from the 7th layer for additional deposition of layers with Hep to form 9 or 10 layers, where PChi or Hep were the final layer of PChi-containing PEM, respectively. PE solution was added on the substrate to prepare every layer and was discarded after 15 min incubation. Subsequently, 0.15 M NaCl solution was used to rinse the surface for 3 × 4 min to remove unbound PE for 3 × 4 min. All PE were prepared at 1 mg mL^{-1} in 0.15 M NaCl solution and adjusted their final pH to 4. Chi was dissolved in 0.05 mol L^{-1} acetic acid solution at 50 °C for 3 h and stirred overnight. Chi-containing PEMs as comparison were based on the assembly of Chi and Hep. The PEMs with X terminal layer were referred as B-$[X/H]_{1.5}$ and with Hep terminal layer were defined as B-$[X/H]_2$, where the term 'B' referred to basal layers comprised of 1−6 layers and LMW*, HMW, or Chi were represented as 'X'.

EDC and NHS were used to covalently crosslink the multilayer based on the protocol established earlier in our group [18,37]. The crosslinked solution was prepared by 50 mg mL^{-1} EDC and 11 mg mL^{-1} NHS in 0.15 M, pH 5 NaCl solution and subsequently added to PEMs to react at 4 °C for 18 h under gentle shaking. The solution was discarded from the crosslinked PEM followed by 3 time rinsing of samples with 0.15 M, pH 8 NaCl solution for 1 h to remove unreacted cross-linker.

2.4. Atomic force microscopy measurement

The investigation of roughness and stiffness of PEMs was carried out by atomic force microscope (AFM, Nanowizard IV, JPK-Instruments, Berlin, Germany) in Quantitative Imaging Mode (QI). Samples were first measured in 0.15 M, pH 7.4 NaCl solution at 20 °C using silicon cantilever (qp-BioT, Nanosensors) in a standard liquid cell (JPK-Instruments). Further topographic and spectroscopic measurements were performed in the liquid cell with temperature stabilization at 37 °C. The analysis of roughness and stiffness were calculated by the software JKP Data Processing V5.0.85 and Gwyddion (Gwyddion V2.49, 64-bit).

2.5. Protein adsorption and release studies

2.5.1. Vitronectin adsorption and desorption

VN was labelled with FITC (referred to as FITC-VN) based on the protocol (Sigma-Aldrich) shown in supporting information. The crosslinked PEMs were fabricated in black 96-well tissue culture plates (TCPS, Greiner). FITC-VN at a concentration of 5 μg mL^{-1} dissolved in phosphate-buffered saline (PBS, pH 7.4) was used for incubating samples at either 25 °C or 37 °C for 1 h. Subsequently, the supernatant was aspirated and transferred to a new black 96-well TCPS. The fluorescence intensity (FI) of the supernatants was measured by fluorometry (FLUOstar Optima, BMG LabTech., Offenburg, Germany) at an excitation wavelength of 488 nm and an emission wavelength of 530 nm to determine the concentration of remaining VN after exposure to PEMs.

After transferring FITC-VN supernatants, PBS (at 4 or 37 °C, pH 7.4) with an amount of 70 μL was used to rinse the PEMs 3 times for removal of excessive VN solution. VN desorption was performed by adding 70 μL PBS to the samples for incubation at 4 °C or 37 °C for 24 h and then transferred to a new black 96 well plate. Then 70 μL 0.2 M NaOH was added and incubated for another 2 h. The amount of desorbed VN from PEMs was determined by collecting supernatants of PBS and NaOH for the measurement of FI. A calibration curve was made from the FI of known concentrations (0.005, 0.05, 0.1, 0.5 and 5 μg mL^{-1}) of FITC-VN for calculation of the amount of adsorbed and desorbed VN.

2.5.2. Release of fibroblast growth factor 2 (FGF-2)

The crosslinked PEMs were prepared in the 96-well plate followed by washing with sterile PBS once. All the surfaces were pre-treated with Dulbecco's modified Eagle's medium (DMEM, Lonza, Walkersville, USA) containing 1 % pen/strep/amphotericin B at 37 °C for 1 h to deactivate unreacted EDC/NHS ester that might be reactive during the following VN adsorption and FGF-2 loading. After DMEM was aspirated, PEMs were incubated in solutions of 5 μg mL^{-1} FGF-2 mixed with 2 μg mL^{-1} VN in 0.15 M, pH 7.4 NaCl at 37 °C for 1 h to allow the loading of FGF-2. Thereafter, the supernatants of FGF-2/VN solutions were collected, and the samples were rinsed once with PBS. Thereafter, 70 μL PBS corresponding to physiological fluids regarding ionic strength and pH value was immediately added to study the release of FGF-2. Half of the supernatant was collected and replaced by fresh PBS after incubation for 2, 4, 6, 8 h at the first day and the following 1–7 days. All the supernatants were stored at −80 °C for further quantification of FGF-2 using a human FGF-basic standard ABTS enzyme-linked immunosorbent assay (ELISA, Peprotech, New Jersey, USA) development kit and ABTS ELISA buffer kit (Peprotech, New Jersey, USA). The use of PBS for release and quantification of FGF-2 was favored for the ELISA assay to avoid any cross-reactivity of antibodies with proteins contained in serum (e.g. growth factors). It was assumed that the PEMs structure is not affected by changing the medium due to the covalent crosslinking and similar ionic strength and same pH of DMEM and PBS to NaCl [32].

2.6. Studies with cells

2.6.1. Cell culture

3T3 mouse embryonic fibroblasts was provided by DSMZ (Deutsche Sammlung von Mikroorganismen und Zellkulturen GmbH, Braunschweig, Germany) and cultured in DMEM supplemented with 10 % fetal bovine serum (FBS, Biochrom AG, Berlin, Germany) and 1 % pen/strep/amphotericin B (BioWhittaker, Lonza, Walkserville, USA) at 37 °C in a humidified 5 % CO_2/95 % air atmosphere using a NuAire DH Autoflow incubator (NuAire Corp., Plymouth, Minnesota, USA). At 80 % confluence, cells were trypsinized by 0.25 % trypsin/0.02 % EDTA (Biochrom AG, Berlin, Germany) solution for 5 min at 37 °C followed by inactivation of trypsin with DMEM containing serum. After the cell suspension was obtained by centrifugation at 500*g* for 5 min, the supernatant was aspirated. The cell pellet was resuspended in DMEM containing 10 % FBS and 1 % pen/strep/amphotericin B. Cell number was manually counted using a Neubauer chamber.

2.6.2. Optimization of VN concentration

The crosslinked PEMs were prepared in the 48-well plate followed by washing with sterile PBS once. All the surfaces were pre-treated with DMEM containing 1 % pen/strep/amphotericin B at 37 °C for 1 h to deactivate unreacted EDC/NHS ester. After aspirating DMEM, 250 μL of VN (at a concentration of 2 or 5 μg mL^{-1} mixed with or without 5 μg mL^{-1} FGF-2 in 0.15 M, pH 7.4 NaCl solution) were coated on PEMs to incubate at 37 °C for 1 h. Thereafter, the FGF-2/VN solutions were discarded, and the surfaces were rinsed with PBS once. 3T3 cells were seeded on the substrates coated with crosslinked PEMs loaded with VN/FGF-2 at a density of 5000 cells per well in 300 μL of DMEM supplemented with low serum (2.5 % FBS). Cells cultured on TCPS in DMEM containing 10 % FBS were used as positive control. On the other hand, soluble FGF-2 at a concentration of 10 ng mL^{-1} in low-serum DMEM (2.5 % FBS) was applied for cells seeded on TCPS coated with VN to compare with PEMs loaded with FGF-2. After 2 days culture, the cell metabolic activity and growth were quantified using Qblue assay (BioChain, Newark, CA, USA). The 10 % of Qblue reagent was added to the medium for reaction at 37 °C for 2 h. After incubation, the 100 μL of supernatant with duplicate were transferred from each sample to the black 96-well plate. The FI of supernatants was measured by fluorometry at a wavelength of 544 nm for excitation and 590 nm for emission.

2.6.3. Cell adhesion studies

After determination of VN concentration, a density of 20,000 cells mL^{-1} of 3 T3 cells were seed on the PEM-coated Nunc Thermanox™ slides (13 mm, Thermo Fisher, NY, USA) pre-adsorbed with VN/FGF-2 that were placed in the 24-well plate in DMEM supplemented with 2.5 % FBS. Cells were incubated for 1 day and fixed with 4 % paraformaldehyde (RotiHistofix, Carl Roth GmbH, Karlsruhe, Germany)

solution for 15 min followed by rinsing PBS twice. Afterwards, cell permeabilization was done using 0.1 % Triton X-100 (Sigma-Aldrich Chemie GmbH, Taufkirchen, Germany) in PBS (v/v) for 10 min. The samples were washed with PBS and blocked the non-specific sites by incubation with 1 % (w/v) bovine serum albumin (BSA, Merck, Darmstadt, Germany)/ 1 % (w/v) glycine (ROTH, Carl Roth GmbH, Karlsruhe, Germany) in PBS at room temperature for 1 h. Focal adhesion was stained with the primary mouse antibody (1:100, Sigma) against vinculin and the secondary Cy2-conjugated goat anti-mouse antibody (1:100, Dianova). Phalloidin CruzFluor 555 (1:1000, Santa Cruz Biotechnology, Heidelberg, Germany) was used to visualize actin cytoskeleton. Cell nuclei were stained with TO-PRO3 (1:500, Invitrogen, Darmstadt, Germany). All the staining on the samples were incubated at room temperature for 30 min followed by 3 times PBS washing. Finally, the samples were mounted on the object slides with Roti-Mount FluorCare (Carl Roth GmbH, Karlsruhe, Germany). Confocal laser scanning microscopy (CLSM 701, Carl Zeiss Micro-Imaging GmbH, Jena, Germany) were used for the measurement of cell number with the 10× objective, cell area with 20× objective, and visualization of focal adhesions, actin and nuclei with 63× oil immersion objective. The images were processed by the ZEN2012 software (Carl Zeiss) and analyzed the cell number and area by ImageJ.

2.6.4. Cell growth

Cell growth was performed by Qblue assay. 3T3 cells were seed on 48-well plated coated with VN/FGF-2-loaded PEMs at a density of 5000 cells per well in DMEM supplemented with 2.5 % FBS and incubated at 37 °C in a 5 % CO_2/95 % air atmosphere. The 10 % of Qblue reagent was added to the medium on day 2 and 4 for reaction at 37 °C for 2 h. After incubation, the 100 μL of supernatant with duplicate were transferred from each sample to the black 96-well plate. The FI of supernatants was measured by fluorometry at a wavelength of 544 nm for excitation and 590 nm for emission.

2.6.5. Cell migration

The sterilized cell migration fences (Aix Scientifics CRO, Aachen, Germany) were inserted into the 24-well plate coated with pre-adsorbed VN/FGF-2 PEMs at 37 °C for 30 min to ensure the attachment of the silicone ring on the surface. 150 μL of 3T3 cell suspension in DMEM supplemented with 2.5 % FBS were seeded in the internal channel of the fence at a density of 20,000 cells per well. The external channel was filled with only DMDM. After 24 h incubation at 37 °C, 5 % CO_2/95 % air atmosphere, the fences were removed. The old medium was removed, and cells were rinsed once with DPBS. Additional 5 μg mL^{-1} of mitomycin C (abcr GmbH, Karlsruhe, Germany) was included in DMEM supplemented with 2.5 % FBS and add to each condition to inhibit cell proliferation for migration study. Cells were incubated for another 24 h and 72 h and washed once with DPBS for fixation using methanol (Carl Roth GmbH, Karlsruhe, Germany). The samples were stained with 10 % (*v*/v) Giemsa (Merck KgaA, Darmstadt, Germany) solution in Milli-Q water for 10 min and subsequently washed with PBS and Milli-Q water. A series of image were photographed along the diameter of the stained area of a cell layer using transmitted light microscope (Nikon ECLIPSE Ti2, Tokyo, Japan). The images were processed using stitching plugin from ImageJ to measure the length of the diameter of the cell layer [38].

2.7. Statistical analysis

All data were performed by Origin Pro 2019 software to obtain a mean value ± standard deviations (SD). The statistical calculation was carried out using a one-way ANOVA with posthoc Turkey's test. The significant difference is indicated as the asterisk when the p value ≤ 0.05. Additionally, the box-whisker plots are presented where applicable. The 25th and 75th percentile, the median (dash) and mean value (empty circle) are illustrated by the box.

3. Results and discussion

3.1. Surface and mechanical properties of multilayers

Since all the PEMs were fabricated and chemically crosslinked at 20 °C, it is important to investigate the effect of size and DS of PNIPAM grafting on Chi during the temperature change from 20 °C to 37 °C on surface properties, like topography and mechanical properties, which are related to protein adsorption, cell adhesion and spreading [39]. Fig. 1A and B represent the wet topography of B-[Chi/H], B-[LMW*/H], and B-[HMW/H] PEMs with either Chi-/LMW*-/HMW- or Hep terminal layers studied by AFM depending on the temperature, respectively. All the PEMs showed an island-like morphology with a roughness (root mean square, Rq) of 1.24–2.46 nm as evaluated in Fig. 1C and Table 1. At 20 °C, the native B-$[Chi/H]_{1.5}$ exhibited the roughest surface while other surfaces were smoother and less granular, which can be explained by the compaction upon addition of smaller molecule of Hep for PEMs with Hep terminal layers and the grafting of PNIPAM for B-[LMW*/H] and B-[HMW/H] PEMs [40,41]. In comparison to the more homogeneous surface of B-[Chi/H], B-[LMW*/H] and B-[HMW/H] PEMs were more inhomogeneous probably due to the bulky structure of LMW* and HMW, which is evident by the rougher and more granular surfaces of their Hep terminal layer also corresponding to their higher dry thickness (Table 1). When PEMs were incubated at 37 °C, surfaces of B-$[Chi/H]_2$ and B-$[HMW/H]_2$ were smoother than at 20 °C. It has been reported that increasing temperature promotes the interdiffusion of polymers and rearrangement of PEMs by breaking the intermolecular interaction (e.g., ionic bonds) between polymers that become more mobile. As a result, a favorable conformation of PEM is reached with a more compact and smoother surface [23,42]. It should be noted that these PEMs were chemically crosslinked with around 40–60 % crosslinking degree that should still permit a certain degree of polymer diffusion (Table 1). In addition, PNIPAM undergoes conformational changes with rising temperature and aggregates resulting in tighter packing and a smoother surface, which is also observed in other PNIPAM-containing PEMs [23,43]. However, B-[LMW*/H] PEMs did not show an alteration of their surface topography during temperature change, probably due to steric hindrance caused by the higher crosslinking degree (54 %) in B-[LMW*/H] PEMs that limits the mobility of PNIPAM chains and other components [44].

To investigate the temperature effect on the mechanical properties of PEM, Young's modulus was measured for different terminal layers as shown in Fig. 1D and Table 1. At 20 °C, the Young's modulus shows a peak of 23 MPa and 24 MPa for B-$[Chi/H]_{1.5}$ and B-$[Chi/H]_2$, respectively, which indicates the stiffest surfaces. The peaks shifted to around 17 MPa for PEMs with LMW* and HMW terminal layers, suggesting PEM involving PNIPAM makes the surface softer because of its higher hydration below LCST [45,46]. The addition of Hep to PEMs indeed stiffened the surfaces, which is correlated to their compact morphology due to diffusion of H inside the PEM increasing ion pairing [41]. Noteworthy, the stiffness is significantly lower for B-$[LMW*/H]_2$ compared to B-$[Chi/H]_2$ and B-$[HMW/H]_2$ ($p \leq 0.05$). This is consistent to the finding that B-$[LMW*/H]_2$ has the most hydrophilic surface of as found by WCA indicating a higher water content of this system. As temperature increased to 37 °C, the stiffness decreased and the peaks of all the surfaces shifted to <10 MPa, indicating overall softer surfaces. Such softening effect on PEMs with elevated temperature was also reported in previous studies [42,47]. Köhler and co-workers suggested a "melting" behavior of the more mobile polymers leading to a softer surface investigating the PSS/PDADMAC multilayer capsules [48,49]. On the other hand, since PNIPAM chains dehydrate and collapse above LCST, the hydrophobic interaction and formation of intramolecular hydrogen bonds of PNIPAM should lead to a stiffer surface [46,50]. Here the LMW* and HMW layers only existed in the terminal bilayers, causing probably only minor effects indicated by relatively stiffer surfaces for B-[LMW*/H] and B-[HMW/H] PEMs compared to B-[Chi/H] PEMs at

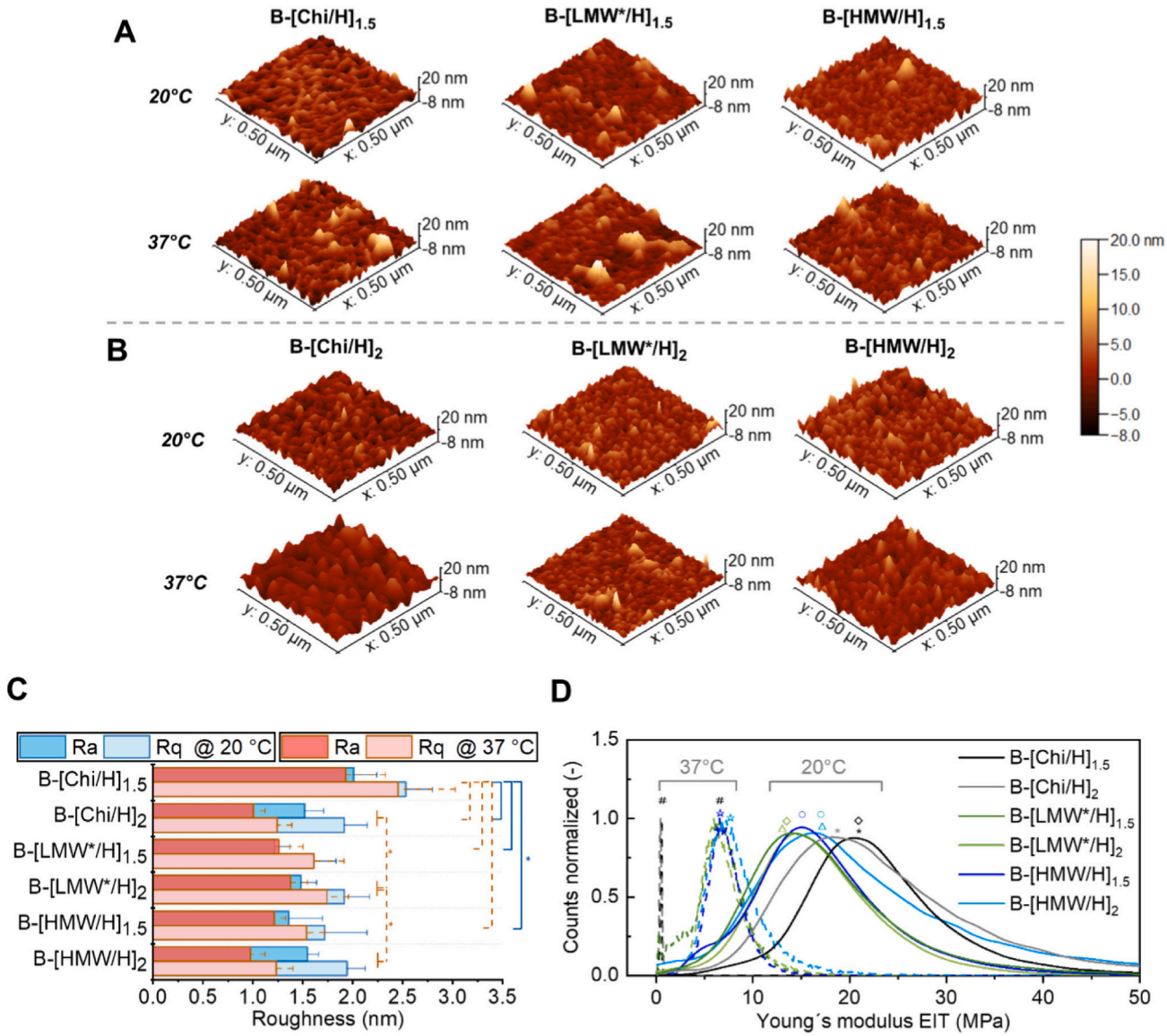

Fig. 1. Surface topography of PEMs with (A) Chi/LMW*/HMW terminal layers and (B) Hep terminal layers at 20 °C (upper row) and 37 °C (bottom row) by atomic force microscopy with 0.5 × 0.5 μm^2 of scan size. (C) Roughness (Ra: average, deep color, Rq: root mean square, light color) of PEMs at 20 °C (blue bar) and 37 °C (red bar). Data represent means ± SD from ten separated lines, *$p \leq 0.05$. (D) Distribution curves of Young's modulus for different PEMs at 20 °C (solid line) and 37 °C (dot line) with 1 × 1 μm^2 of scan size. All the measurements were done under exposure to 0.15 M, pH 7.4 NaCl solution. Data represent means ± SD across the whole scan size, $p \leq 0.05$ (the symbols of *, ○, △, ⋄ indicate the significant difference at 20 °C and ☆, # at 37 °C.).

Table 1
Surface properties and mechanical properties for PEMs exposed to 0.15 M, pH 7.4 NaCl at 20 °C and 37 °C. Data of chemical crosslinking degree, thickness, water contact angle (WCA, data from previous study [32]) and AFM data such as stiffness and root mean square (Rq) after rinsing with PBS and DMEM at pH 7.4. (means ± SD).

Surface property	Crosslinking degree (%)	Thickness (nm)	WCA (°)		Rq (nm)		Stiffness (MPa)	
			20 °C	37 °C	20 °C	37 °C	20 °C	37 °C
B-[Chi/H]$_{1.5}$		8.76 ± 1.38	37.84 ± 4.35	37.55 ± 2.32	2.54 ± 0.27	2.46 ± 0.58	23.25 ± 8.66	0.49 ± 0.08
B-[Chi/H]$_2$	59	10.53 ± 0.79	29.98 ± 7.81	30.76 ± 8.13	1.92 ± 0.23	1.25 ± 0.15	24.23 ± 12.39	0.46 ± 0.15
B-[LMW*/H]$_{1.5}$		8.40 ± 0.39	27.78 ± 1.96	32.77 ± 3.63	1.61 ± 0.22	1.62 ± 0.30	17.82 ± 8.48	6.61 ± 2.98
B-[LMW*/H]$_2$	54	11.66 ± 0.96	10.51	14.48 ± 4.10	1.92 ± 0.25	1.74 ± 0.22	19.96 ± 6.67	7.23 ± 2.73
B-[HMW/H]$_{1.5}$		9.67 ± 0.25	33.60 ± 1.18	37.48 ± 1.65	1.72 ± 0.42	1.54 ± 0.18	17.50 ± 7.57	7.35 ± 2.30
B-[HMW/H]$_2$	39	11.38 ± 0.50	27.12 ± 1.45	29.56 ± 1.90	1.95 ± 0.18	1.24 ± 0.17	24.83 ± 20.64	8.61 ± 4.00

37 °C. These observations are related to results of wetting studies in Table S1 showing that PEMs containing PNIPAM have higher water contact angles at 37 °C than at 20 °C. Combining these results, it confirms that HMW is more mobile and able to change its conformation within the B-[HMW/H] PEMs resulting in stiffer surfaces compared to slightly softer surfaces for B-[LMW*/H] PEMs at 37 °C.

3.2. Effect of temperature on vitronectin adsorption and desorption

VN is a plasma protein important for blood coagulation after injury, cell adhesion and tissue remodeling [51]. VN has been used for coating substrata playing a dominant role in maintaining self-renewal and promoting adhesion and proliferation of hPSC in vitro via the specific ligation of $\alpha_v\beta_3$ and $\alpha_v\beta_5$ integrins [33]. The conformational change of PNIPAM with temperature leading to changes of wettability may promote protein adsorption and subsequent cell adhesion [26,52]. Here FITC-labelled VN (named as FITC-VN) was used to study its adsorption on PEMs with different terminal layers and compared to the control surface TCPS at 20 °C and 37 °C as shown in Fig. 2A and B. The amount of adsorbed VN was calculated based on the calibration curve shown in Fig. S1. It was observed that substantially higher quantities of VN adsorbed on all PEMs with about 275–300 ng cm^{-2} at 37 °C in comparison to <100 ng cm^{-2} at 20 °C. At 20 °C, the lowest amount of VN was found on B-[LMW*/H]$_2$, corresponding to the most hydrophilic surface (WCA ≈ 10°, see Table 1) due to prominent hydration effect of LMW* and H. As the temperature increased to 37 °C, the amount of adsorbed VN on B-[LMW*/H] and B-[HMW/H] PEMs was similar to B-[Chi/H] PEMs, which is related to the dehydrated state of PNIPAM leading to less hydrophilic surfaces (Table 1), and thus promoting protein adsorption [53]. Here the temperature plays a key role in protein adsorption as an external factor. Hydrophobic interaction is likely to promote protein adsorption due to the release of water from the interface at higher temperature causing an entropy gain [54]. Jackler et al. observed not only higher adsorption but also more penetration of protein on/into the PEM of Si-PEI-PSS-[PAH-PSS]$_5$ at 42 °C than at 22 °C using staphylococcal nuclease with a MW of 17 kDa [55]. They attributed higher protein adsorption at higher temperature to the entropy gain by the release of counterions and the complexation between proteins and polymer chains. In our case, large Chi or PChi might allow the interpenetration of VN with a MW of about 52 kDa accompanied by the complexation with the polymers in the PEMs regarding higher mobility of molecules at higher temperature. In addition, the amount of around 300 ng cm^{-2} of VN adsorbed on TCPS was found in another study [56].

According to the higher amount of adsorbed VN at 37 °C, VN pre-adsorbed on PEMs at 37 °C was selected to determine the protein desorption at 4 °C and 37 °C as shown in Fig. 2C. After 24 h desorption in PBS, a higher amount of 6–12 ng cm^{-2} of VN was released from PEMs at 37 °C compared to negligible release at 4 °C correlated to the mobility of protein at different temperatures, which means that lower temperature stabilizes adsorption of VN. Following the extraction by NaOH at 37 °C to hydrolyze FITC-VN remained on the surfaces, higher cumulative amount of desorbed VN was found at 37 °C than at 4 °C. Considering physiological condition at 37 °C, it is important to know how much VN can be retained on the surfaces at 37 °C to support cell adhesion. B-[LMW*/H]$_{1.5}$ and B-[HMW/H]$_{1.5}$ released the highest amount of VN around 30 ng cm^{-2}. By contrast, only 10–15 ng cm^{-2} was desorbed from their Hep terminal layers. Although protein adsorption and desorption can also be thermally controlled by PNIPAM surface, it seems that Hep plays a dominant role in the association with VN through the specific Hep-binding domain of VN [57]. It should be noted that not all the amount of protein could be depleted from the surface by NaOH regarding the specific binding affinity to Hep that also explains almost 95 % desorbed quantity of VN from TCPS having no specific interaction with VN (Fig. S1B) [58]. B-[HMW/H]$_2$ retained more VN on the surface compared to B-[LMW*/H]$_2$ possibly due to higher amount of Hep remained in B-[HMW/H]$_2$ to binding with VN as confirmed in the previous study by washing step with physiological buffers at pH 7.4 [32]. As mentioned in our previous study, the binding of Hep and protein with Hep-binding domains requires their steric interaction [59]. However, a higher density of PNIPAM in B-[LMW*/H]$_2$ PEM may cause a steric hindrance against change of its conformation as indicated by the AFM studies. This could block some binding sites of Hep that hinder its interaction with VN. As 250 ng cm^{-2} of VN has shown to be the minimal surface density required for hPSC adhesion and growth, B-[HMW/H]$_2$ is preferable for long-term cell culture as a bioactive surface [60].

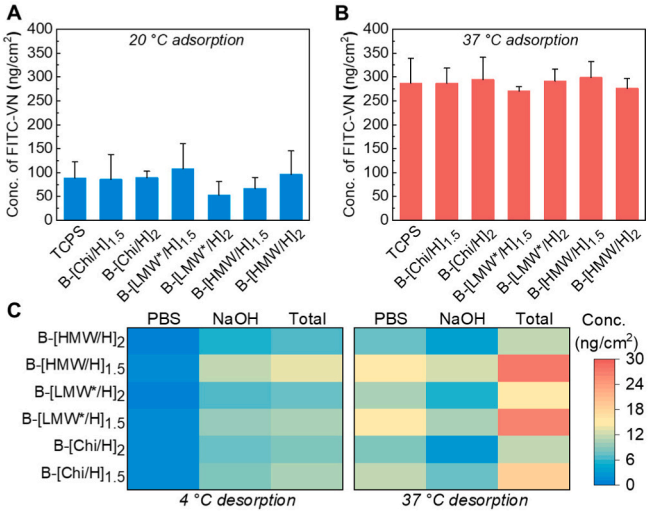

Fig. 2. Amount of FITC-VN adsorbed on Chi/LMW*/HMW or Hep terminated PEMs at (A) 20 °C and (B) 37 °C. (C) Desorption of FITC-VN pre-adsorbed on PEMs at 37 °C in PBS for 24 h at 4 °C (left) and 37 °C (right), succeeded by 2 h extraction in 0.2 M NaOH solution for obtaining cumulative amount of desorbed VN. The unit of VN concentration was transferred from μg mL^{-1} to ng cm^{-2} (= 1000 × 70/0.34) using the volume (70 μL) of the solution added in the 96 well plate with the surface area of 0.34 cm^{-2}.

3.3. Optimization of VN concentration for FGF-2 loading regarding cell reactions

Both VN and FGF-2 possess a high affinity to Hep due to the presence of Hep-binding domains [6]. Thus, the amount of VN should be controlled to avoid the competition between them to bind to heparin that may affect the activity of immobilized FGF-2 and thus cell adhesion, migration, and growth. Fig. 3A illustrates simultaneous incubation of PEM in VN and FGF-2 solutions to immobilize FGF-2 named as iFGF-2. Low serum medium containing 2.5 % FBS was used for iFGF-2-loaded PEMs during cell culture [19]. Here incubation of 2 or 5 μg mL^{-1} VN on B-[Chi/H]$_2$ was studied using 3T3 cells for mitogenic activity that can be promoted by FGF-2. For comparison as a control, the soluble form of FGF-2 (sFGF-2) was added exogenously in low-serum medium to VN-adsorbed TCPS. The growth of 3T3 cells on the surfaces after 2 days of cultivation was detected with Qblue assay that measures FI for the metabolic activity of viable cells as shown in Fig. 3B. Stronger FI was observed for all VN-adsorbed surfaces compared to weaker FI for plain TCPS using 10 % FBS in the medium. Increasing concentration of VN from 2 to 5 μg mL^{-1} slightly decreased FI on B-[Chi/H]$_2$. When B-[Chi/H]$_2$ was loaded with iFGF-2, the FI was visibly higher than non-loaded B-[Chi/H]$_2$, corresponding to denser population of cells observed from the phase contrast images in Fig. 3C, indicating promoting effect of iFGF-2 on cell growth. The concentration of VN did not significantly affect FI of cells on TCPS cultured with sFGF-2. However, slightly higher FI is observed for iFGF-2-loaded B-[Chi/H]$_2$ when adsorbed with 2 μg mL^{-1} VN than with 5 μg mL^{-1} VN, implicating some competition between VN and iFGF-2 binding to H.

This study is the first report to explore the potential of VN involved in PEM for cell culture. Our study confirmed that the amount of VN adsorbed on the PEMs was around 250–275 ng cm^{-2} from 5 μg mL^{-1} of VN, similar to a study that demonstrates VN could also increase the expression of FGF2 receptor [34]. Although the activation of integrin is thought to be necessary for sustained activity of FGFR-2, an early study has argued that high concentration (> 5 μg mL^{-1}) of VN might inhibit cell adhesion and growth when FGF-2 was immobilized on the surface

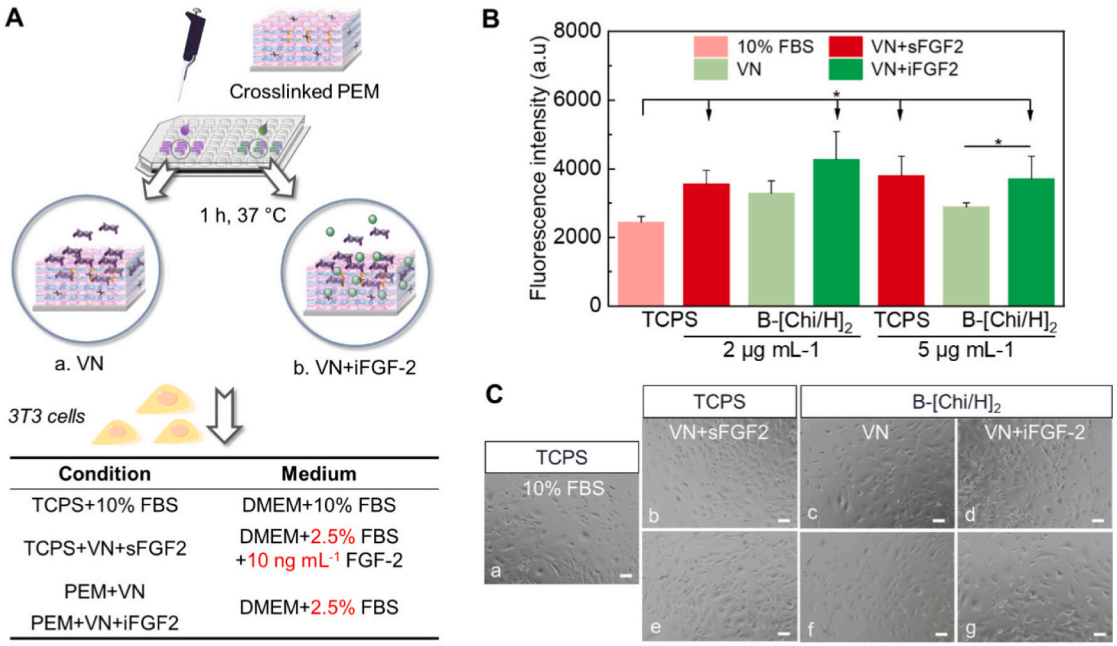

Condition	Medium
TCPS+10% FBS	DMEM+10% FBS
TCPS+VN+sFGF2	DMEM+2.5% FBS +10 ng mL^{-1} FGF-2
PEM+VN PEM+VN+iFGF2	DMEM+2.5% FBS

Fig. 3. (A) Illustration of adsorption process of VN on PEMs accompanying (a) with or (b) without immobilization of FGF-2 (iFGF-2) for 1 h at 37 °C. 3T3 cells were seeded on the surfaces after removing FGF-2/VN solution in culture medium DMEM supplemented with 2.5 % FBS. Cells seeded on TCPS in DMEM containing 10 % FBS or on TCPS pre-adsorbed with VN in DMEM containing 2.5 % FBS and 10 ng mL^{-1} of soluble FGF-2 (sFGF2) were compared as control. (B) The intensity of cell growth detected using Qblue assay and (C) the cell morphology for PEMs pre-adsorbed with 2 (b – d) or 5 (e – g) μg mL^{-1} of VN and loaded with or without FGF-2 after 2-day culture. Data represent means ± SD, $n = 4$, $^*p \leq 0.05$.

[6]. This study also shows 5 μg mL^{-1} VN seemed to compete with iFGF-2 to bind Hep in some but not substantial extent. Therefore, a concentration of 2 μg mL^{-1} VN adsorbed on PEMs is more suitable for this study to promotes iFGF-2 activity in a matrix-bound manner that even surpasses the effect of sFGF-2 on cell growth.

3.4. Release of FGF-2

After optimization of the VN concentration, the ability of FGF-2 uptake and release in B-[Chi/H]$_2$ and B-[HMW/H]$_2$ was studied by ELISA. The calibration curve of the FGF-2 concentration at 10–1000 pg mL^{-1} presents a logarithmic relationship to the absorbance at the wavelength of 405 nm in Fig. 4A. The percentage of cumulative release of FGF-2 from both PEMs at 37 °C was calculated over 7 days as shown in Fig. 4B. For both of PEMs, a high-level release of nearly 20 % was observed for the first 16 h, followed by a slower release at different rates. Notably, the release was faster from B-[Chi/H]$_2$ and reached 40 % of the initial loaded FGF-2 (609 ng mL^{-1}) at day 4 compared to about 30 % release of initial loaded amount (707 ng mL^{-1}) from B-[HMW/H]$_2$. From day 5 to 7, <5 % of FGF-2 was released from both the PEMs.

It was found previously that thicker, more swollen and less crosslinked PEM can take up more FGF-2 [2,61]. Our previous study has shown that B-[HMW/H]$_2$ is slightly thicker and more hydrated than B-[Chi/H]$_2$ at 20 °C. Nevertheless, the thickness and hydration of B-[HMW/H]$_2$ is supposed to be decreased based on the collapsed PNIPAM chains at 37 °C. The hydrophobic interaction between PNIPAM and FGF-2 might account for the higher uptake of FGF-2 in B-[HMW/H]$_2$ [26]. Additionally, Hep has high affinity to FGF-2 mainly mediated by iduronate-2-sulfates and *N*-sulfate groups while marginally by carboxylic groups and hydroxyl groups in H through ionic interaction and hydrogen bonding [11]. Since the chemical crosslinking is higher for B-[Chi/H]$_2$ (60 %) than B-[HMW/H]$_2$ (40 %) according to our previous study [32], less free carboxylic groups and a more restricted mobility are reducing the capability to bind FGF-2 for B-[Chi/H]$_2$. In contrast, a lower crosslinked B-[HMW/H]$_2$ allows FGF-2 to access Hep and penetrate inside the PEM [2]. On the other hand, Table S1 estimates that the

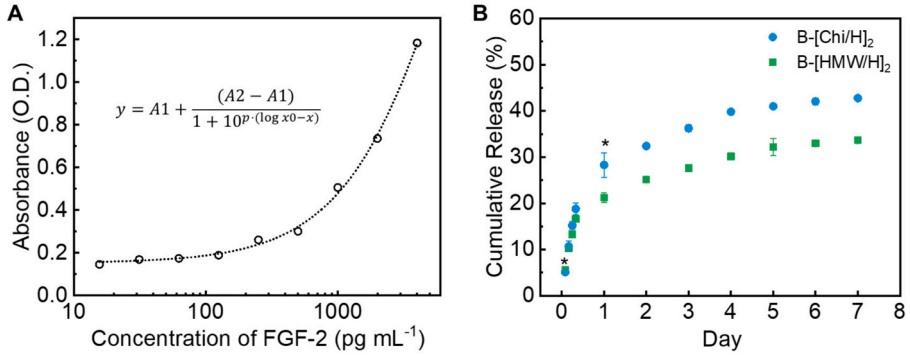

Fig. 4. (A) Calibration curve for FGF-2 at the concentration of 10–4000 pg mL^{-1} with a logarithmic relationship to the absorbance at the wavelength of 405 nm. (A1 = −53.64, A2 = 2.20, $R^2 = 0.99$) (B) Percentage of cumulative release of FGF-2 from PEMs of B-[Chi/H]$_2$ and B-[HMW/H]$_2$ over the 7 days. Data represent means ± SD, $n = 4$, $^*p \leq 0.05$.

release profiles were fit the most accordingly to Higuchi model with the highest correlation coefficient (R^2), suggesting the release mechanism was governed by the diffusion of entrapped FGF-2 out of these PEM that is in well agreement with other studies [2,19]. The release rate of FGF-2 is slower from B-[HMW/H]$_2$ (2.43 ng/day) and faster from B-[Chi/H]$_2$ (3.27 ng/day). Principally, a higher crosslinking degree of the polymer network should delay the release [61]. Our findings show opposite results that could be explained by the hydrophobic effect of PNIPAM at 37 °C to bind FGF-2 in B-[HMW/H]$_2$. Thus, the release of FGF-2 can be sustained by presence of PNIPAM in PEM.

3.5. Cell adhesion studies

The cell adhesion process involves focal adhesion formation where the networks of actin cytoskeleton is connected to ECM proteins through integrins that results in biochemical and mechanical signal transduction into the cell and consequently regulating cell spreading, migration, growth and differentiation [62]. In addition, FGF-2 also promotes these processes through the crosstalk between FGFR and integrins since they co-localize in the focal adhesion contacts [63]. Here, the impact of iFGF-2 loading on VN-adsorbed PEMs for adhesion and spreading of 3T3 cells after 1 day culture was studied by staining nuclei for quantification of cell number, vinculin for formation of focal adhesion and actin cytoskeleton for cell spreading. Thermanox as cell culture-treated plastic slides was used as a positive control for cell culture in medium supplemented with 10 % FBS. The low-serum medium containing sFGF2 for VN-adsorbed Thermanox was used for another comparison. In the absence of iFGF-2, Fig. 5A shows the lowest cell number on VN-adsorbed B-[Chi/H]$_2$, while cell number was higher on B-[HMW/H]$_2$ and both Thermanox surfaces. The average cell area was similar on both PEMs as presented in Fig. 5B. CLSM images shown in Fig. 5C visualize that the formation of actin cytoskeleton is observed in cells, indicating good attachments of cells to all the surfaces. For PEMs, a rich formation of focal adhesions was observed at the cell periphery where vinculin is located at the end of actin fibers, however, lesser actin fiber formation was present in cells on B-[Chi/H]$_2$ than on B-[HMW/H]$_2$.

The presence of vinculin-positive focal adhesions and actin stress fiber formation on all VN-adsorbed surfaces indicate the ligation between VN and integrins like $\alpha_V\beta_3$, which activates the intracellular signaling pathway and thereby regulating cell adhesion and spreading [52]. Confirmed by the results of VN adsorption/desorption, both B-[Chi/H]$_2$ and B-[HMW/H]$_2$ have high binding affinity to VN at 37 °C resulting in similar cell spreading. In addition, the higher cell number on B-[HMW/H]$_2$ might be attributed to less wettable surface and increased

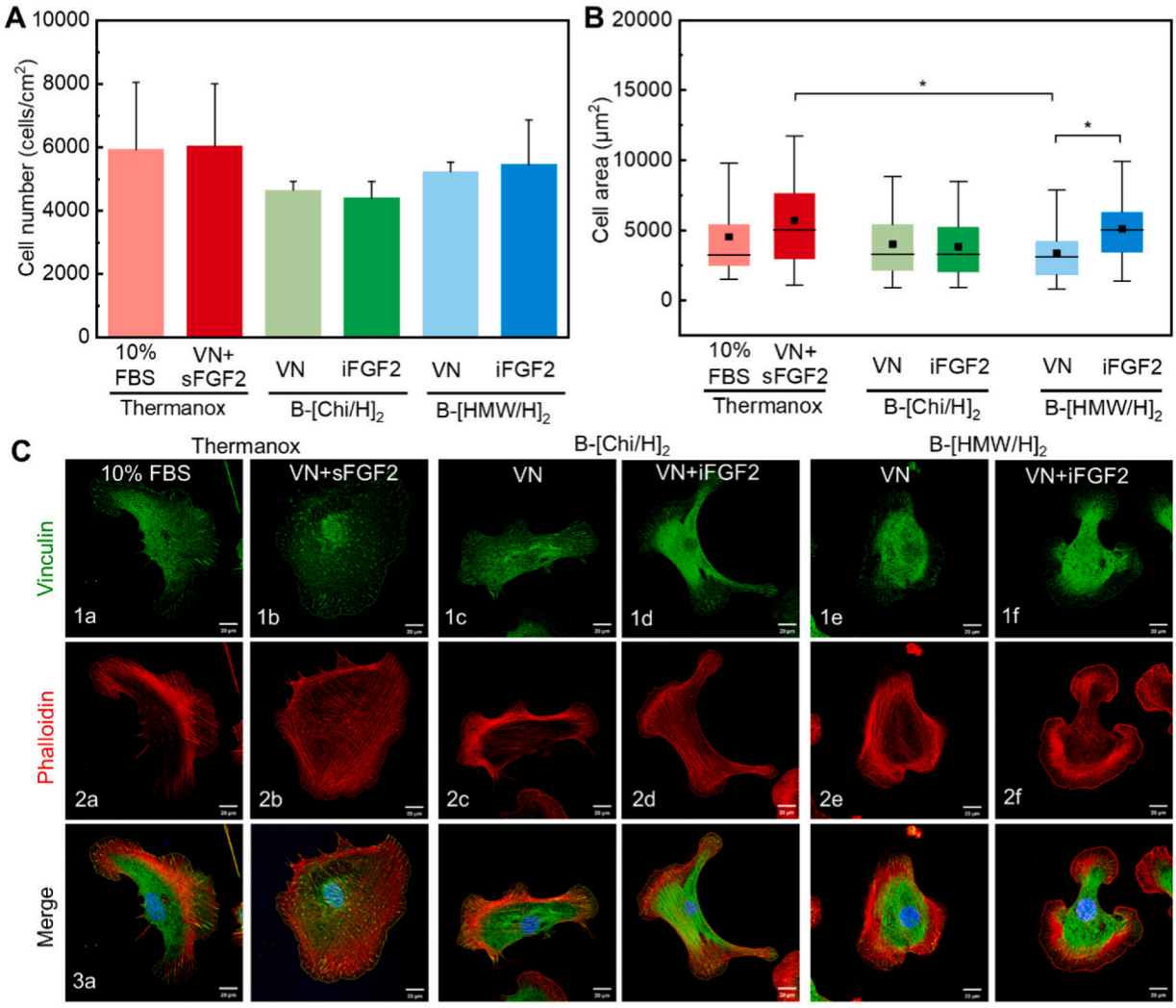

Fig. 5. Quantification of 3T3 cell (A) number and (B) area on different VN-adsorbed PEMs loaded with or without iFGF-2 after 1-day incubation. (C) Confocal laser scanning microscopy images of staining of vinculin (green, 1a–1f), phalloidin (red, 2a–2f) and nuclei (blue, 3a–3f) of cells. Cells seeded on Thermanox in DMEM containing 10 % FBS or on Thermanox pre-adsorbed with VN in DMEM containing 2.5 % FBS and 10 ng mL^{-1} sFGF-2 were compared as control. Scale bar: 20 μm. Data represent means ± SD, $n = 4$, *$p \leq 0.05$.

stiffness at 37 °C compared to B-[Chi/H]$_2$. Mechanical properties of biomaterials such as stiffness play an important role in cell adhesion and spreading through mechano-sensing by integrins that regulate RhoA/ROCK signaling pathway for cell adhesion and spreading [64]. Stiffer surfaces induce assembly of actin fiber and formation of focal adhesion, which is displayed by more cell adhesion and spreading on B-[HMW/H]$_2$ than on the softer surface of B-[Chi/H]$_2$ [65].

Loading iFGF-2 on PEMs did not result in any significant difference in quantity of cell adhesion. Notably, cells became larger on B-[HMW/H]$_2$ comparable to fibroblasts on VN-adsorbed Thermanox in the presence of sFGF2, which is indicated by more pronounced actin networks at the leading edge of cells and reveals the formation of well-defined lamellipodium also as a sign of cell migration [66]. This is attributed to more active iFGF-2 within the B-[HMW/H]$_2$ than B-[Chi/H]$_2$ at day 1, where reorganization of actin cytoskeleton can be induced by FGF-2 through the activation of Rho GTPases family like Rac and Cdc42 [67]. In addition, FGFR-2 and VN integrins $\alpha_V\beta_3$ and $\alpha_V\beta_5$ have been reported to regulate cooperatively through many convergent signaling pathways such as MAPK/ERK pathway for cell spreading [6,68]. In comparison, more actin fibers and vinculin distributed across the ventral cell side on VN-adsorbed Thermanox that links to firmly attached and less mobile cells even in the presence of sFGF-2, probably due to stiffer surface than PEMs and lower efficacy of soluble compared to immobilized FGF-2.

3.6. Cell proliferation and migration

The mitogenic activity of iFGF-2 loaded PEMs for the proliferation of 3T3 cells was visualized in Fig. 6A and investigated by FI of Qblue assay for evaluation of metabolic activity after 2- and 4-day cultivation as shown in Fig. 6B. The trend of cell proliferation on day 2 roughly corresponded to cell number counted at day 1. Likewise, B-[Chi/H]$_2$ PEMs showed the lowest cell number and FI while no significant difference was observed between B-[HMW/H]$_2$ PEMs and TCPS. On day 4, more cells were observed on all the surfaces. Remarkedly, loading iFGF-2 on B-[HMW/H]$_2$ exhibited the most pronounced cell proliferation compared to non-loaded B-[HMW/H]$_2$ and both B-[Chi/H]$_2$ PEMs. It was surprising to observe that cell growth is slightly better on non-loaded B-[Chi/H]$_2$ than iFGF-2-loaded one. Cell growth did not take advantage of the sFGF-2 supplemented in low-serum medium for VN-adsorbed TCPS in contrast to significantly more cell growth on plain TCPS supplemented with 10 % FBS.

Our results show the surfaces coated with VN alone enhances cell proliferation due to integrin ligation, the activation of focal adhesion kinase and subsequent MAPK pathway [69]. In addition, the specific interaction of iFGF-2 with Hep in PEMs is supposed to be in a matrix-bound manner to stabilize and prolong the half-life of FGF-2 by formation of a complex with FGFR-2 and integrin that induces intracellular signaling [12,19]. However, a burst release of about 35 % and 40 % of FGF-2 from B-[Chi/H]$_2$ on day 2 and day 4 is related to lower amount of iFGF-2 bound on the PEM matrix and corresponds well to lower FI and hence proliferative effect on cells. By contrast, more iFGF-2 preserved on B-[HMW/H]$_2$ exhibited an exceptional bioactivity promoting cell proliferation. On the other hand, due to degradation of sFGF-2, cell proliferation was inhibited by insufficient amount of sFGF-2 and unavailable crosstalk between FGFR-2 and integrin [15].

The migratory effect of FGF-2 on cells by activation of Rho GTPases family including Rac and Cdc42 is crucial for embryonic development, tissue regeneration and wound healing [19,67]. Here, migration of 3T3 cells was further studied on PEMs by addition of mitomycin C to inhibit cell outgrowth that interferes the estimation on position of migration of a cell layer. Fig. 6C presents the overall large expansion of cell layers about 10.5–11.5 mm on all substrates compared to TCPS with migration

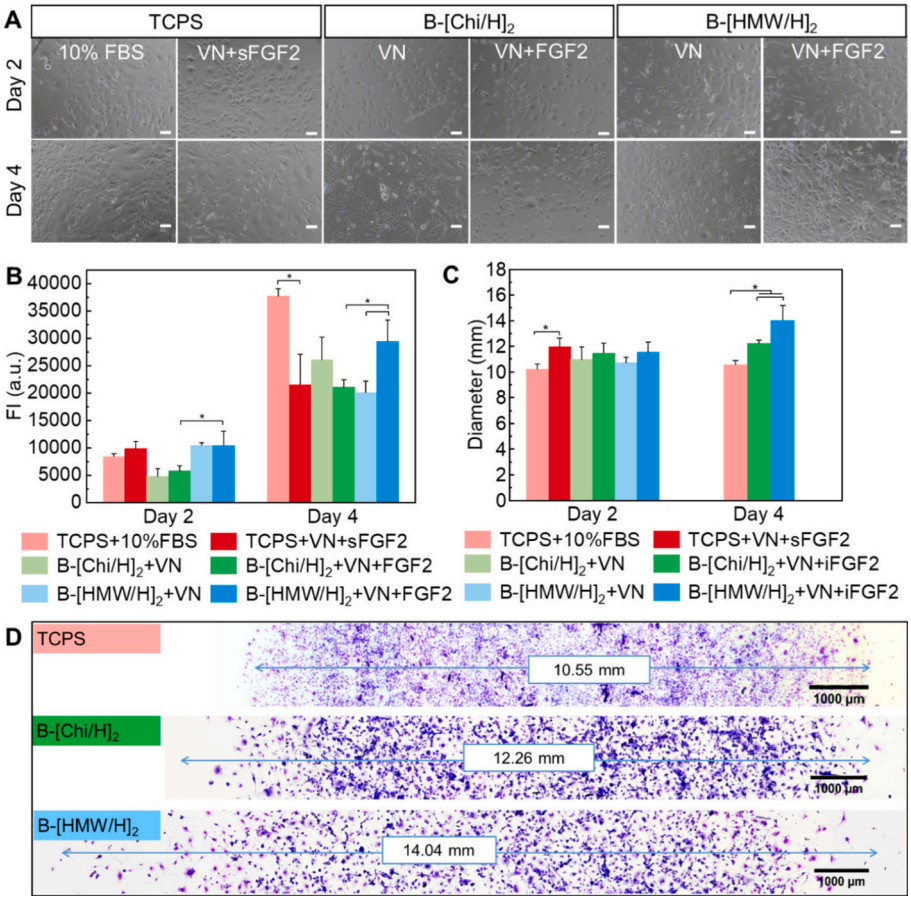

Fig. 6. (A) Phase contrast images of cell morphology and (B) metabolic activity evaluated by Qblue assay to determine the proliferation of 3T3 cells on the different surfaces after 2- and 4- day cultivation. Data represent means ± SD, $n = 6$, $^*p \leq 0.05$. Scale bar: 100 μm. Length of 3T3 cell migration on (C) VN-adsorbed PEMs loaded with or without iFGF-2 on day 2 and loaded with FGF-2 on day 4 in 2.5 % FBS medium containing 5 μg mL^{-1} mitomycin C. Migration fence was inserted for TCPS over the culture period to be used as control in 10 % FBS medium. (D) Photographs of cells stained with 10 % Giemsa on VN-adsorbed PEMs loaded with iFGF-2 on day 4. Scale bar: 1000 μm. Data represents means ± SD, $n = 4$, *p ≤ 0.05.

fence at day 2. A slightly larger cell expansion can be observed on iFGF-2-loaded PEMs with 1 mm more diameter compared to unloaded PEMs. Considering the presentation of FGF-2 activity, cells were continuing cultured on iFGF-2-loaded PEMs until day 4. The migration of the cell layer was significantly promoted to about a diameter of 14 mm on B-[HMW/H]$_2$ as shown in Fig. 6C and D. However, iFGF-2 did not show obvious effect on B-[Chi/H]$_2$ where diameter of the cell layer was only around 12 mm.

The synergistic effect of FGFR-2 and ligation of integrins to VN regulates cell migration via activation of MAPK/ERK activity [6]. The sign of migratory activity of iFGF-2 in the cell adhesion study after 1 day culture has been observed for B-[HMW/H]$_2$. Cell migration stood out on B-[HMW/H]$_2$ regarding the formation of lamellipodium at the leading edge and disassembly of focal adhesion at cell rear (Fig. 5C). Myosin-generated forces transmitted by focal adhesions from actin cytoskeleton to ECM induce a tracking force to pull cell forward [70]. The disassembly of focal adhesion regulated by the inactivation of vinculin and depolymerization of actin filament are evident by weak signal of vinculin and actin at the cell rear [70,71]. During cell migration, proteolysis and remodeling of ECM is required mainly by proteinases like urokinase-type plasminogen activator that can be activated by stimulation of FGF-2 and regulated by VN [3,56]. The presentation of iFGF-2 was better sustained on the surface of B-[HMW/H]$_2$ leading to superior cell migration over the course of 4 days. It seems that the migration was limited on B-[Chi/H]$_2$ probably due to fast release of iFGF-2. Taking all the results together, PEM comprised of bioactive H and HMW efficiently promotes not only cell proliferation but also cell migration in the presence of matrix-bound FGF-2. Both processes are important in wound healing, but also neovascularization and show the versatility of the combination of these PEs with FGF-2 and VN.

4. Conclusion

This study demonstrates a cost-effective and facile LbL technique for coating biomaterials and tissue culture ware allowing the establishment of synergistic bioactive effects of adhesive proteins like VN and growth factors such as FGF-2 to direct cell behaviors when bound to multilayers made of thermoresponsive PNIPAM-*grafted*-chitosan and bioactive heparin. In particular, using high molecular weight of PNIPAM grafted on chitosan as polycation combined with polyanion heparin allows PEM formation and modification with thermoresponsiveness. Heparin plays an important role in retention of adsorbed VN layer and binding of FGF-2 while dehydrated PNIPAM chains at 37 °C enhances the stabilization of VN and FGF-2 in the PEM to promote cell adhesion, proliferation, and migration in a long-term culture of fibroblasts in this study but also potentially for other type of cells like hPSC. Such surface coatings might be interesting for application in culture and programming stem cells in vitro but also in applications related to wound healing when growth and migration of cells like endothelial cells, fibroblasts and keratinocytes is required for tissue regeneration.

CRediT authorship contribution statement

Yi-Tung Lu: Methodology, Validation, Investigation, Data curation, Writing – original draft. **Pei-Tzu Hung:** Investigation, Formal analysis. **Kui Zeng:** Methodology, Writing – review & editing. **Matthias Menzel:** Methodology, Resources, Writing – review & editing. **Christian E.H. Schmelzer:** Methodology, Resources, Writing – review & editing. **Kai Zhang:** Funding acquisition, Writing – review & editing. **Thomas Groth:** Supervision, Funding acquisition, Project administration, Conceptualization, Writing – review & editing.

Declaration of competing interest

The authors declare that they have no known competing financial interests or personal relationships that could have appeared to influence the work reported in this paper.

Data availability

Data will be made available on request.

Acknowledgement

This work was funded by the International Graduate School AGRIPOLY supported by the European Regional Development Fund (ERDF) and the Federal State Saxony-Anhalt, and Deutsche Forschungsgemeinschaft under grant agreements Gr 1290/12-1 and ZH 546/3-1. Dr. Kui Zeng thanks China Scholarship Council for his PhD grant. Aspects of diagrams adapted with permission from Servier Medical Art library (http://smart.servier.com/), available under Creative Commons license.

Appendix A. Supplementary data

Supplementary data to this article can be found online at https://doi.org/10.1016/j.bioadv.2023.213589.

References

[1] M. Qu, X. Jiang, X. Zhou, C. Wang, Q. Wu, L. Ren, J. Zhu, S. Zhu, P. Tebon, W. Sun, A. Khademhosseini, Stimuli-responsive delivery of growth factors for tissue engineering, Adv. Healthc. Mater. 9 (2020), e1901714, https://doi.org/10.1002/adhm.201901714.

[2] A. Hautmann, D. Kedilaya, S. Stojanović, M. Radenković, C.K. Marx, S. Najman, M. Pietzsch, J.F. Mano, T. Groth, Free-standing multilayer films as growth factor reservoirs for future wound dressing applications, Biomater. Adv. 142 (2022), 213166, https://doi.org/10.1016/j.bioadv.2022.213166.

[3] B. Boilly, A.S. Vercoutter-Edouart, H. Hondermarck, V. Nurcombe, X. Le Bourhis, FGF signals for cell proliferation and migration through different pathways, Cytokine Growth Factor Rev. 11 (2000) 295–302, https://doi.org/10.1016/s1359-6101(00)00014-9.

[4] A.N. Sohi, H. Naderi-Manesh, M. Soleimani, E.R. Yasaghi, H.K. Manjili, S. Tavaddod, S. Nojehdehi, Synergistic effect of co-immobilized FGF-2 and vitronectin-derived peptide on feeder-free expansion of induced pluripotent stem cells, Mater. Sci. Eng. C Mater. Biol. Appl. 93 (2018) 157–169, https://doi.org/10.1016/j.msec.2018.07.072.

[5] A. Novais, E. Chatzopoulou, C. Chaussain, C. Gorin, The potential of FGF-2 in craniofacial bone tissue engineering: a review, Cells 10 (2021), https://doi.org/10.3390/cells10040932.

[6] M. Rusnati, E. Tanghetti, P. Dell'Era, A. Gualandris, M. Presta, alphavbeta3 integrin mediates the cell-adhesive capacity and biological activity of basic fibroblast growth factor (FGF-2) in cultured endothelial cells, Mol. Biol. Cell 8 (1997) 2449–2461, https://doi.org/10.1091/mbc.8.12.2449.

[7] S. Mori, Y. Takada, Crosstalk between Fibroblast Growth Factor (FGF) receptor and integrin through direct integrin binding to FGF and resulting integrin-FGF-FGFR ternary complex formation, Med. Sci. 1 (2013) 20–36, https://doi.org/10.3390/medsci1010020.

[8] I. Ding, A.M. Peterson, Half-life modeling of basic fibroblast growth factor released from growth factor-eluting polyelectrolyte multilayers, Sci. Rep. 11 (2021) 9808, https://doi.org/10.1038/s41598-021-89229-w.

[9] M. Garcia-Maya, A.A. Anderson, C.E. Kendal, A.V. Kenny, L.C. Edwards-Ingram, A. Holladay, J.L. Saffell, Ligand concentration is a driver of divergent signaling and pleiotropic cellular responses to FGF, J. Cell. Physiol. 206 (2006) 386–393, https://doi.org/10.1002/jcp.20483.

[10] Á. Apáti, T. Berecz, B. Sarkadi, Calcium signaling in human pluripotent stem cells, Cell Calcium 59 (2016) 117–123, https://doi.org/10.1016/j.ceca.2016.01.005.

[11] Y. Yang, Y.-T. Lu, K. Zeng, T. Heinze, T. Groth, K. Zhang, Recent progress on cellulose-based ionic compounds for biomaterials, Adv. Mater. (2020), e2000717, https://doi.org/10.1002/adma.202000717.

[12] A. Weltrowski, M.-L. Da Silva Almeida, D. Peschel, K. Zhang, S. Fischer, T. Groth, Mitogenic activity of sulfated chitosan and cellulose derivatives is related to protection of FGF-2 from proteolytic cleavage, Macromol. Biosci. 12 (2012) 740–750, https://doi.org/10.1002/mabi.201100518.

[13] D. Peschel, K. Zhang, N. Aggarwal, E. Brendler, S. Fischer, T. Groth, Synthesis of novel celluloses derivatives and investigation of their mitogenic activity in the presence and absence of FGF2, Acta Biomater. 6 (2010) 2116–2125, https://doi.org/10.1016/j.actbio.2009.12.032.

[14] R. Anouz, A. Repanas, E. Schwarz, T. Groth, Novel surface coatings using oxidized glycosaminoglycans as delivery systems of Bone Morphogenetic Protein 2 (BMP-2) for bone regeneration, Macromol. Biosci. 18 (2018), e1800283, https://doi.org/10.1002/mabi.201800283.

[15] J.M. Silva, R.L. Reis, J.F. Mano, Biomimetic extracellular environment based on natural origin polyelectrolyte multilayers, Small 12 (2016) 4308–4342, https://doi.org/10.1002/smll.201601355.

[16] J. Borges, J.F. Mano, Molecular interactions driving the layer-by-layer assembly of multilayers, Chem. Rev. 114 (2014) 8883–8942, https://doi.org/10.1021/cr400531v.
[17] L. Richert, F. Boulmedais, P. Lavalle, J. Mutterer, E. Ferreux, G. Decher, P. Schaaf, J.-C. Voegel, C. Picart, Improvement of stability and cell adhesion properties of polyelectrolyte multilayer films by chemical cross-linkin, Biomacromolecules 5 (2004) 284–294, https://doi.org/10.1021/bm0342281.
[18] G. Apte, A. Repanas, C. Willems, A. Mujtaba, C.E.H. Schmelzer, A. Raichur, F. Syrowatka, T. Groth, Effect of different crosslinking strategies on physical properties and biocompatibility of freestanding multilayer films made of alginate and chitosan, Macromol. Biosci. 19 (2019), e1900181, https://doi.org/10.1002/mabi.201900181.
[19] J. Almodóvar, S. Bacon, J. Gogolski, J.D. Kisiday, M.J. Kipper, Polysaccharide-based polyelectrolyte multilayer surface coatings can enhance mesenchymal stem cell response to adsorbed growth factors, Biomacromolecules 11 (2010) 2629–2639, https://doi.org/10.1021/bm1005799.
[20] R. Mhanna, J. Becher, M. Schnabelrauch, R.L. Reis, I. Pashkuleva, Sulfated alginate as a mimic of sulfated glycosaminoglycans: binding of growth factors and effect on stem cell behavior, Adv. Biosyst. 1 (2017), e1700043, https://doi.org/10.1002/adbi.201700043.
[21] L. Xu, X. Zhang, Z. Chu, H. Wang, Y. Li, X. Shen, L. Cai, H. Shi, C. Zhu, J. Pan, D. Pan, Temperature-responsive multilayer films based on block copolymer-coated silica nanoparticles for long-term release of Favipiravir, ACS Appl. Nano Mater. 4 (2021) 14014–14025, https://doi.org/10.1021/acsanm.1c03334.
[22] Y.-T. Lu, P.-T. Hung, K. Zeng, C. Woelk, B. Fuhrmann, K. Zhang, T. Groth, Surface properties and bioactivity of PNIPAM-grafted-chitosan/chondroitin multilayers, Smart Mater. Med. 4 (2023) 356–367, https://doi.org/10.1016/j.smaim.2022.11.008.
[23] A. Osypova, C.-A. Fustin, C.-M. Pradier, J. Landoulsi, S. Demoustier-Champagne, Factors impacting protein adsorption on layer-by-layer assembled stimuli-responsive thin films, Eur. Polym. J. 95 (2017) 195–206, https://doi.org/10.1016/j.eurpolymj.2017.08.019.
[24] F. Doberenz, K. Zeng, C. Willems, K. Zhang, T. Groth, Thermoresponsive polymers and their biomedical application in tissue engineering - a review, J. Mater. Chem. B 8 (2020) 607–628, https://doi.org/10.1039/c9tb02052g.
[25] M. Prawatborisut, S. Jiang, J. Oberländer, V. Mailänder, D. Crespy, K. Landfester, Modulating protein corona and materials–cell interactions with temperature-responsive materials, Adv. Funct. Mater. 32 (2022) 2106353, https://doi.org/10.1002/adfm.202106353.
[26] J. Kobayashi, Y. Arisaka, N. Yui, Y. Akiyama, M. Yamato, T. Okano, Effect of temperature changes on serum protein adsorption on thermoresponsive cell-culture surfaces monitored by a quartz crystal microbalance with dissipation, Int. J. Mol. Sci. 19 (2018), https://doi.org/10.3390/ijms19051516.
[27] M. Cao, Y. Wang, X. Hu, H. Gong, R. Li, H. Cox, J. Zhang, T.A. Waigh, H. Xu, J. R. Lu, Reversible thermoresponsive peptide-PNIPAM hydrogels for controlled drug delivery, Biomacromolecules 20 (2019) 3601–3610, https://doi.org/10.1021/acs.biomac.9b01009.
[28] C.A. Kavanagh, T.A. Gorelova, I.I. Selezneva, Y.A. Rochev, K.A. Dawson, W. M. Gallagher, A.V. Gorelov, A.K. Keenan, Poly(N-isopropylacrylamide) copolymer films as vehicles for the sustained delivery of proteins to vascular endothelial cells, J. Biomed. Mater. Res. A 72 (2005) 25–35, https://doi.org/10.1002/jbm.a.30192.
[29] J.C. Garbern, E. Minami, P.S. Stayton, C.E. Murry, Delivery of basic fibroblast growth factor with a pH-responsive, injectable hydrogel to improve angiogenesis in infarcted myocardium, Biomaterials 32 (2011) 2407–2416, https://doi.org/10.1016/j.biomaterials.2010.11.075.
[30] E. Smith, J. Yang, L. McGann, W. Sebald, H. Uludag, RGD-grafted thermoreversible polymers to facilitate attachment of BMP-2 responsive C2C12 cells, Biomaterials 26 (2005) 7329–7338, https://doi.org/10.1016/j.biomaterials.2005.05.060.
[31] K. Zeng, F. Doberenz, Y.-T. Lu, J.P. Nong, S. Fischer, T. Groth, K. Zhang, Synthesis of thermoresponsive PNIPAM-grafted cellulose sulfates for bioactive multilayers via layer-by-layer technique, ACS Appl. Mater. Interfaces 14 (2022) 48384–48396, https://doi.org/10.1021/acsami.2c12803.
[32] Y.-T. Lu, K. Zeng, B. Fuhrmann, C. Woelk, K. Zhang, T. Groth, Engineering of stable cross-linked multilayers based on thermo-responsive PNIPAM-grafted-chitosan/heparin to tailor their physiochemical properties and biocompatibility, ACS Appl. Mater. Interfaces 14 (2022) 29550–29562, https://doi.org/10.1021/acsami.2c05297.
[33] T.J. Rowland, L.M. Miller, A.J. Blaschke, E.L. Doss, A.J. Bonham, S.T. Hikita, L. V. Johnson, D.O. Clegg, Roles of integrins in human induced pluripotent stem cell growth on Matrigel and vitronectin, Stem Cells Dev. 19 (2010) 1231–1240, https://doi.org/10.1089/scd.2009.0328.
[34] R. Tsou, F.F. Isik, Integrin activation is required for VEGF and FGF receptor protein presence on human microvascular endothelial cells, Mol. Cell. Biochem. 224 (2001) 81–89, https://doi.org/10.1023/a:1011947301849.
[35] T. Crouzier, L. Fourel, T. Boudou, C. Albigès-Rizo, C. Picart, Presentation of BMP-2 from a soft biopolymeric film unveils its activity on cell adhesion and migration, Adv. Mater. 23 (2011) H111–H118, https://doi.org/10.1002/adma.201004637.
[36] R. Anouz, T. Selekere, A. Hautmann, C. Husteden, M. Menzel, C. Woelk, C.E. H. Schmelzer, T. Groth, Intrinsically cross-linked ECM-like multilayers for BMP-2 delivery promote osteogenic differentiation of cells, Adv. Mater. Interfaces 10 (2023) 2201596, https://doi.org/10.1002/admi.202201596.
[37] M.S. Niepel, F. Almouhanna, B.K. Ekambaram, M. Menzel, A. Heilmann, T. Groth, Cross-linking multilayers of poly-l-lysine and hyaluronic acid: effect on mesenchymal stem cell behavior, Int. J. Artif. Organs 41 (2018) 223–235, https://doi.org/10.1177/0391398817752598.
[38] S. Preibisch, S. Saalfeld, P. Tomancak, Globally optimal stitching of tiled 3D microscopic image acquisitions, Bioinformatics 25 (2009) 1463–1465, https://doi.org/10.1093/bioinformatics/btp184.
[39] M. Rahmati, E.A. Silva, J.E. Reseland, C.A. Heyward, H.J. Haugen, Biological responses to physicochemical properties of biomaterial surface, Chem. Soc. Rev. 49 (2020) 5178–5224, https://doi.org/10.1039/d0cs00103a.
[40] M. Lundin, F. Solaqa, E. Thormann, L. Macakova, E. Blomberg, Layer-by-layer assemblies of chitosan and heparin: effect of solution ionic strength and pH, Langmuir 27 (2011) 7537–7548, https://doi.org/10.1021/la200441u.
[41] N. Aggarwal, Modulating cell behaviour through biomimetic multilayers of natural and semi-synthetic glycosaminoglycans, in: Universitäts- und Landesbibliothek Sachsen-Anhalt, 2014, https://doi.org/10.25673/1129.
[42] P. Nazaran, V. Bosio, W. Jaeger, D.F. Anghel, R.V. Klitzing, Lateral mobility of polyelectrolyte chains in multilayers, J. Phys. Chem. B 111 (2007) 8572–8581, https://doi.org/10.1021/jp068768e.
[43] T. Fujie, J.Y. Park, A. Murata, N.C. Estillore, M.C.R. Tria, S. Takeoka, R. C. Advincula, Hydrodynamic transformation of a freestanding polymer nanosheet induced by a thermoresponsive surface, ACS Appl. Mater. Interfaces 1 (2009) 1404–1413, https://doi.org/10.1021/am900111r.
[44] J.A. Jaber, J.B. Schlenoff, Polyelectrolyte multilayers with reversible thermal responsivity, Macromolecules 38 (2005) 1300–1306, https://doi.org/10.1021/ma0485235.
[45] G. Liu, G. Zhang, Collapse and swelling of thermally sensitive poly(N-isopropylacrylamide) brushes monitored with a quartz crystal microbalance, J. Phys. Chem. B 109 (2005) 743–747, https://doi.org/10.1021/jp046903m.
[46] E. Maza, C. von Bilderling, M.L. Cortez, G. Díaz, M. Bianchi, L.I. Pietrasanta, J. M. Giussi, O. Azzaroni, Layer-by-layer assembled microgels can combine conflicting properties: switchable stiffness and wettability without affecting permeability, Langmuir 34 (2018) 3711–3719, https://doi.org/10.1021/acs.langmuir.8b00047.
[47] A.S. Vikulina, Y.G. Anissimov, P. Singh, V.Z. Prokopović, K. Uhlig, M.S. Jaeger, R. von Klitzing, C. Duschl, D. Volodkin, Temperature effect on the build-up of exponentially growing polyelectrolyte multilayers. An exponential-to-linear transition point, Phys. Chem. Chem. Phys. 18 (2016) 7866–7874, https://doi.org/10.1039/c6cp00345a.
[48] K. Köhler, H. Möhwald, G.B. Sukhorukov, Thermal behavior of polyelectrolyte multilayer microcapsules: 2. Insight into molecular mechanisms for the PDADMAC/PSS system, J. Phys. Chem. B 110 (2006) 24002–24010, https://doi.org/10.1021/jp062907a.
[49] R. Mueller, K. Köhler, R. Weinkamer, G. Sukhorukov, A. Fery, Melting of PDADMAC/PSS capsules investigated with AFM force spectroscopy, Macromolecules 38 (2005) 9766–9771, https://doi.org/10.1021/ma0513057.
[50] M.H. Futscher, M. Philipp, P. Müller-Buschbaum, A. Schulte, The role of backbone hydration of poly(N-isopropyl acrylamide) across the volume phase transition compared to its monomer, Sci. Rep. 7 (2017) 17012, https://doi.org/10.1038/s41598-017-17272-7.
[51] D.I. Leavesley, A.S. Kashyap, T. Croll, M. Sivaramakrishnan, A. Shokoohmand, B. G. Hollier, Z. Upton, Vitronectin–master controller or micromanager? IUBMB Life 65 (2013) 807–818, https://doi.org/10.1002/iub.1203.
[52] T. Groth, G. Altankov, A. Kostadinova, N. Krasteva, W. Albrecht, D. Paul, Altered Vitronectin receptor (αv integrin) function in fibroblasts adhering on hydrophobic glass, J. Biomed. Mater. Res. 44 (1999) 341–351, https://doi.org/10.1002/(SICI)1097-4636(19990305)44:3<341:AID-JBM13>3.0.CO;2-H.
[53] A. Osypova, D. Magnin, P. Sibret, A. Aqil, C. Jérôme, C. Dupont-Gillain, C.-M. Pradier, S. Demoustier-Champagne, J. Landoulsi, Dual stimuli-responsive coating designed through layer-by-layer assembly of PAA-b-PNIPAM block copolymers for the control of protein adsorption, Soft Matter 11 (2015) 8154–8164, https://doi.org/10.1039/c5sm01545f.
[54] I. Kiesel, M. Paulus, J. Nase, S. Tiemeyer, C. Sternemann, K. Rüster, F.J. Wirkert, K. Mende, T. Büning, M. Tolan, Temperature-driven adsorption and desorption of proteins at solid-liquid interfaces, Langmuir 30 (2014) 2077–2083, https://doi.org/10.1021/la404884a.
[55] G. Jackler, C. Czeslik, R. Steitz, C.A. Royer, Spatial distribution of protein molecules adsorbed at a polyelectrolyte multilayer, Phys. Rev. E Stat. Nonlinear Soft Matter Phys. 71 (2005) 41912, https://doi.org/10.1103/PhysRevE.71.041912.
[56] G. Toromanov, D. Gugutkov, J. Gustavsson, J. Planell, M. Salmerón-Sánchez, G. Altankov, Dynamic behavior of Vitronectin at the cell-material Interface, ACS Biomater. Sci. Eng. 1 (2015) 927–934, https://doi.org/10.1021/acsbiomaterials.5b00147.
[57] I. Capila, R.J. Linhardt, Heparin-protein interactions, Angew. Chem. Int. Ed. 41 (2002) 390–412, https://doi.org/10.1002/1521-3773(20020201)41:3<390:AID-ANIE390>3.0.CO;2-B.
[58] J.L. Bohnert, T.A. Horbett, Changes in adsorbed fibrinogen and albumin interactions with polymers indicated by decreases in detergent elutability, J. Colloid Interface Sci. 111 (1986) 363–377, https://doi.org/10.1016/0021-9797(86)90040-8.
[59] N. Aggarwal, N. Altgärde, S. Svedhem, G. Michanetzis, Y. Missirlis, T. Groth, Tuning cell adhesion and growth on biomimetic polyelectrolyte multilayers by variation of pH during layer-by-layer assembly, Macromol. Biosci. 13 (2013) 1327–1338, https://doi.org/10.1002/mabi.201300153.
[60] L.Y.W. Yap, J. Li, I.Y. Phang, L.T. Ong, J.Z.-E. Ow, J.C.H. Goh, V. Nurcombe, J. Hobley, A.B.H. Choo, S.K.W. Oh, S.M. Cool, W.R. Birch, Defining a threshold surface density of vitronectin for the stable expansion of human embryonic stem cells, Tissue Eng. C Methods 17 (2011) 193–207, https://doi.org/10.1089/ten.tec.2010.0328.

[61] M. Kumorek, O. Janoušková, A. Höcherl, M. Houska, E. Mázl-Chánová, N. Kasoju, L. Cuchalová, R. Matějka, D. Kubies, Effect of crosslinking chemistry of albumin/heparin multilayers on FGF-2 adsorption and endothelial cell behavior, Appl. Surf. Sci. 411 (2017) 240–250, https://doi.org/10.1016/j.apsusc.2017.03.193.
[62] W.H. Goldmann, Role of vinculin in cellular mechanotransduction, Cell Biol. Int. 40 (2016) 241–256, https://doi.org/10.1002/cbin.10563.
[63] G.E. Plopper, H.P. McNamee, L.E. Dike, K. Bojanowski, D.E. Ingber, Convergence of integrin and growth factor receptor signaling pathways within the focal adhesion complex, Mol. Biol. Cell 6 (1995) 1349–1365, https://doi.org/10.1091/mbc.6.10.1349.
[64] R.G. Wells, The role of matrix stiffness in regulating cell behavior, Hepatology 47 (2008) 1394–1400, https://doi.org/10.1002/hep.22193.
[65] J. Blacklock, A. Vetter, A. Lankenau, D. Oupický, H. Möhwald, Tuning the mechanical properties of bioreducible multilayer films for improved cell adhesion and transfection activity, Biomaterials 31 (2010) 7167–7174, https://doi.org/10.1016/j.biomaterials.2010.06.002.
[66] S. Tojkander, G. Gateva, P. Lappalainen, Actin stress fibers–assembly, dynamics and biological roles, J. Cell Sci. 125 (2012) 1855–1864, https://doi.org/10.1242/jcs.098087.
[67] J.G. Lee, E.P. Kay, Cross-talk among Rho GTPases acting downstream of PI 3-kinase induces mesenchymal transformation of corneal endothelial cells mediated by FGF-2, Invest. Ophthalmol. Vis. Sci. 47 (2006) 2358–2368, https://doi.org/10.1167/iovs.05-1490.
[68] S. Klein, F.G. Giancotti, M. Presta, S.M. Albelda, C.A. Buck, D.B. Rifkin, Basic fibroblast growth factor modulates integrin expression in microvascular endothelial cells, Mol. Biol. Cell 4 (1993) 973–982, https://doi.org/10.1091/mbc.4.10.973.
[69] Y.-J. Jin, I. Park, I.-K. Hong, H.-J. Byun, J. Choi, Y.-M. Kim, H. Lee, Fibronectin and vitronectin induce AP-1-mediated matrix metalloproteinase-9 expression through integrin α(5)β(1)/α(v)β(3)-dependent Akt, ERK and JNK signaling pathways in human umbilical vein endothelial cells, Cell. Signal. 23 (2011) 125–134, https://doi.org/10.1016/j.cellsig.2010.08.012.
[70] J.L. Bays, K.A. DeMali, Vinculin in cell-cell and cell-matrix adhesions, Cell. Mol. Life Sci. 74 (2017) 2999–3009, https://doi.org/10.1007/s00018-017-2511-3.
[71] J. Lehtimäki, M. Hakala, P. Lappalainen, Actin filament structures in migrating cells, Handb. Exp. Pharmacol. 235 (2017) 123–152, https://doi.org/10.1007/164_2016_28.